

Chapter 2

Polarized Light

Abstract Detailed analysis of light emitted from excited atomic states provides an efficient key to the understanding of many atomic collision processes. The mathematical description of coherent electromagnetic radiation is briefly reviewed, including light polarization, the Stokes vector parameterization, and the Poincaré sphere. The electric dipole radiation pattern emitted from an excited P state is then discussed and related to the scattering amplitudes for excitation of the atomic state. The connection between light polarization and parameters characterizing the atomic state and the electron charge cloud is discussed in some detail, including experimental geometries for their determination. Finally, the effects due to loss of full coherence and non-conservation of atomic reflection symmetry are considered.

2.1 Polarization of Coherent Electromagnetic Radiation

2.1.1 Maxwell's Theory of Electromagnetic Radiation

According to Maxwell, the following set of equations yields a satisfactory description of electric and magnetic phenomena:

$$\nabla \cdot \mathbf{E}(\mathbf{r}, t) = \rho(\mathbf{r}, t)/\epsilon, \quad (2.1a)$$

$$\nabla \cdot \mathbf{B}(\mathbf{r}, t) = 0, \quad (2.1b)$$

$$\nabla \times \mathbf{E}(\mathbf{r}, t) = -\frac{\partial \mathbf{B}(\mathbf{r}, t)}{\partial t}, \quad (2.1c)$$

$$\nabla \times \mathbf{B}(\mathbf{r}, t) = \mu \mathbf{J}(\mathbf{r}, t) - \mu\epsilon \frac{\partial \mathbf{E}(\mathbf{r}, t)}{\partial t}. \quad (2.1d)$$

Here, $\mathbf{E}(\mathbf{r}, t)$ and $\mathbf{B}(\mathbf{r}, t)$ are the time-dependent electric and magnetic fields at the point \mathbf{r} in space, $\rho(\mathbf{r}, t)$ and $\mathbf{J}(\mathbf{r}, t)$ are the charge and current densities, ϵ is the permittivity, and μ is the permeability of the material, respectively.

For the purpose of this book, it is sufficient to consider the case where both ρ and \mathbf{J} vanish, $\epsilon \approx \epsilon_0$, and $\mu \approx \mu_0$, where $\epsilon_0 = 8.85410^{-12} \text{C}^2/\text{Nm}^2$ and $\mu_0 =$

$1/(\epsilon_0 c^2)$, with $c = 299\,792\,458$ m/s being the speed of light in vacuum. These values are sufficiently accurate for air under low and normal pressures. Applying the curl operation to (2.1c), using the identity

$$\nabla \times (\nabla \times \mathbf{f}) = \nabla(\nabla \cdot \mathbf{f}) - (\nabla \cdot \nabla) \mathbf{f} \quad (2.2)$$

together with (2.1a), and interchanging the space and time derivatives in (2.1d) yield the well-known wave equation

$$\square \mathbf{E}(\mathbf{r}, t) = \left(\frac{\partial^2}{\partial x^2} + \frac{\partial^2}{\partial y^2} + \frac{\partial^2}{\partial z^2} - \frac{1}{c^2} \frac{\partial^2}{\partial t^2} \right) \mathbf{E}(\mathbf{r}, t) = 0. \quad (2.3)$$

Starting with the curl operation on (2.1d), the partial differential equation (2.3) for the electric field $\mathbf{E}(\mathbf{r}, t)$ may also be derived for the magnetic field $\mathbf{B}(\mathbf{r}, t)$. Using standard vector analysis, one can verify that

$$\mathbf{E}(\mathbf{r}, t) = \mathbf{E}_0 \exp[i(\mathbf{k} \cdot \mathbf{r} - \omega t)] , \quad (2.4a)$$

$$\mathbf{B}(\mathbf{r}, t) = \mathbf{B}_0 \exp[i(\mathbf{k} \cdot \mathbf{r} - \omega t)] , \quad (2.4b)$$

with complex amplitude vectors \mathbf{E}_0 and \mathbf{B}_0 are solutions for a “monochromatic plane wave” with a single angular frequency $\omega = 2\pi\nu$, provided that

$$\omega = ck. \quad (2.5)$$

Here, $k = |\mathbf{k}| = 2\pi/\lambda$ is the magnitude of the wavevector \mathbf{k} , $\lambda = c/\nu$ is the wavelength, and ν is the frequency.

Throughout this book, we will assume that such a monochromatic plane wave is a sufficiently accurate approximation to the true wave packet that is obtained by a Fourier integral over different frequencies. Since the wave packet is generally produced by dipole radiation from excited atoms or molecules, this requires that the light detector is far enough away from the source to neglect the spherical character of the wave. Finally, we note that only the real parts of the solutions represent the physical electric and magnetic fields, respectively.

We are now in a position to show the transversality of the fields as well as the orthogonality of \mathbf{E} and \mathbf{B} . Using the vanishing divergence (see (2.1a), (2.1b)), we immediately obtain

$$\mathbf{E}_0 \cdot \mathbf{k} = 0 , \quad (2.6a)$$

$$\mathbf{B}_0 \cdot \mathbf{k} = 0 . \quad (2.6b)$$

Furthermore, (2.1b) yields

$$\mathbf{k} \times \mathbf{E}_0 = \omega \mathbf{B}_0 . \quad (2.7)$$

Consequently, the triple $(\mathbf{E}_0, \mathbf{B}_0, \mathbf{k})$ forms a mutually orthogonal right-hand system of vectors with $|\mathbf{B}_0| = |\mathbf{E}_0|/c$.

2.1.2 The Polarization Ellipse

Without loss of generality, we may choose the positive direction of the z -axis along the wavevector \mathbf{k} , i.e.,

$$\mathbf{k} = k \hat{\mathbf{z}}, \quad (2.8)$$

see Fig. 2.1a. With a proper choice of zero time, the time dependence of the electric field at a fixed point on the z -axis may thus be written in the form

$$E_x(t) = E_{x0} \cos(\omega t), \quad (2.9a)$$

$$E_y(t) = E_{y0} \cos(\omega t - \delta), \quad (2.9b)$$

with $E_{x0}, E_{y0} > 0$. Equation (2.9) show that the electric vector traces out an ellipse in time, as shown in Fig. 2.1b. We notice especially the following values of $\delta = 0, \pi/2, \pi, 3\pi/2$, see Fig. 2.1c. The first and third picture correspond to purely linearly polarized light, while some degree of circular polarization is found in the regions in between, $0 < \delta < \pi$ and $\pi < \delta < 2\pi$. In particular, if $\delta = \pi/2$ or $3\pi/2$ and the amplitudes in the x and y directions are the same, we have fully circularly polarized light. Following the notation of classical optics [1], we use the term *right-hand-circular* polarization (RHC) when the electric vector moves *clockwise*, as seen by an observer looking *toward* the light source, as is the case for $\delta = 3\pi/2$. Similarly, the term *left-hand-circular* polarization (LHC) is used when the electric vector moves *counterclockwise*, in the same geometry (e.g., $\delta = \pi/2$).

Since different conventions are used in the literature, we shall briefly elaborate on the connection to concepts such as photon helicity, see Fig. 2.1d. This shows the variation along the z -axis of the electric vector at a fixed time, for RHC and LHC polarized light, respectively. Thus, RHC corresponds to a corkscrew-shaped surface for the electric vector in space. In this picture, no explicit reference to the direction to the light source is required, since a corkscrew is the same whether one screws in or out. For LHC polarization, the surface turns the opposite way. In the photon picture of light, RHC corresponds to a *negative* photon helicity; i.e., loosely speaking, each photon carries one unit of angular momentum \hbar , pointing in the backward direction. Similarly, LHC photons have *positive* helicity, each one carrying one unit of \hbar , pointing forward.

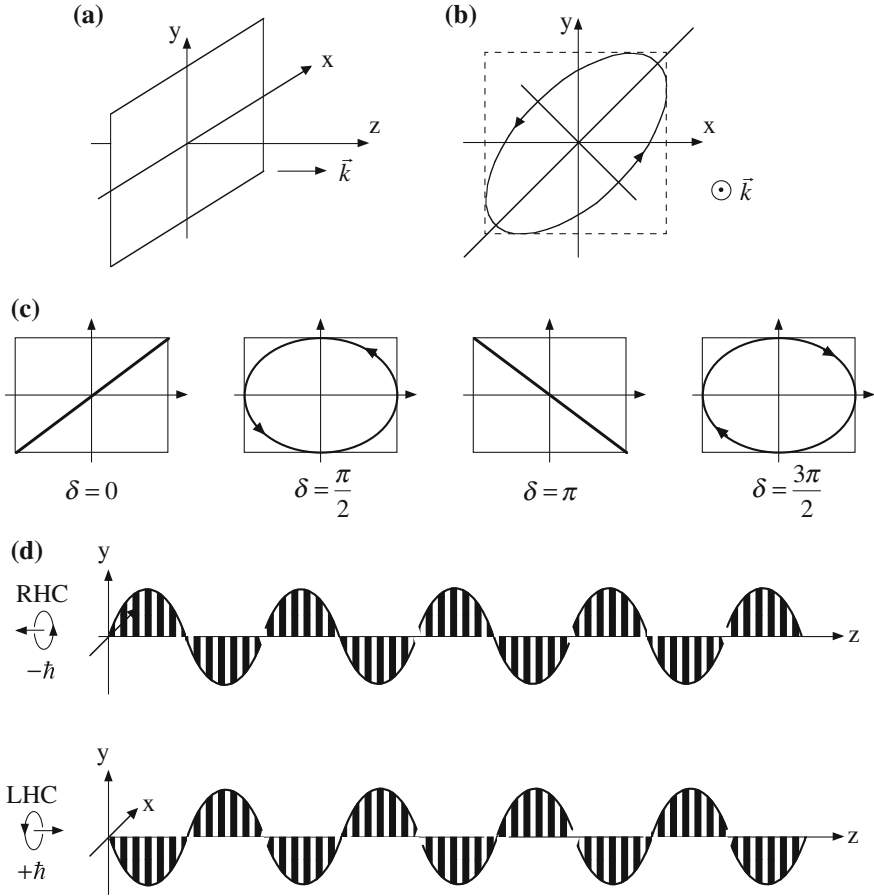


Fig. 2.1 **a** Choice of coordinate system, with the positive z -axis in the direction of the wavevector \vec{k} of the light wave. **b** The endpoint of the electric vector \vec{E} traces out an ellipse in the xy plane. **c** Shape of the polarization ellipse for selected values of the phase angle δ . **d** For fixed time, the electric vector forms a corkscrew surface in space for RHC polarization, while for LHC polarization, the surface turns the other way. The corresponding helicities in the photon picture are also indicated.

2.1.3 Parameterization of Polarization: Stokes Vectors

A complete, quantitative, and operational characterization of the polarization state of a light ray was introduced by Stokes [2]. For this purpose, we here assume access to perfect linear and circular polarizers and refer to standard textbooks [1] for a discussion of their actual realization and procedures for determination of and correction for imperfections. For a given ray of light, in our case specified by (2.9), four Stokes parameters (s_0, s_1, s_2, s_3) may be determined from intensity measurements of the light transmitted through polarizers set in a systematic way:

- (i) We denote by s_0 the total intensity, proportional to the time average of the squared amplitudes of the electric vector components, i.e.,

$$s_0 = \frac{1}{2}(E_{xo}^2 + E_{yo}^2), \quad (2.10a)$$

where the factor $\frac{1}{2}$ originates from averaging the term $\cos^2(\omega t)$ over time. This intensity is also equal to the sum of the two intensities transmitted through a polarizer set at any two mutually orthogonal transmission directions.

- (ii) We denote by s_1 the difference in intensities transmitted through a linear polarizer with its transmission direction parallel to the x -axis and y -axis, respectively, i.e.,

$$s_1 = \frac{1}{2}(E_{xo}^2 - E_{yo}^2). \quad (2.10b)$$

- (iii) We denote by s_2 the difference in intensities transmitted through a linear polarizer with its transmission direction set at angles of 45° and -45° , respectively, with respect to the x -axis. A little algebra (Exercise 2.1) shows that

$$s_2 = E_{xo}E_{yo} \cos \delta. \quad (2.10c)$$

- (iv) Finally, we denote by s_3 the difference in intensities transmitted through a circular polarizer with its transmission set for RHC and LHC polarizations, respectively. Again, a little algebra (Exercise 2.1) shows that

$$s_3 = -E_{xo}E_{yo} \sin \delta. \quad (2.10d)$$

We note from (2.10) the relation

$$s_1^2 + s_2^2 + s_3^2 = s_0^2. \quad (2.11)$$

In cases where only the polarization state and not the total intensity is of interest, the dimensionless Stokes vector $\mathbf{P} = (P_1, P_2, P_3)$ with components defined by

$$P_i = s_i/s_0; \quad i = 1, 2, 3 \quad (2.12)$$

is useful. According to (2.11), \mathbf{P} is a unit vector, i.e.,

$$P_1^2 + P_2^2 + P_3^2 = 1. \quad (2.13)$$

Other notations may be found in the literature, in particular [3]

$$I = s_0, \quad M = s_1, \quad C = s_2, \quad S = s_3, \quad (2.14a)$$

and [4,5]

$$\eta_1 = P_2, \eta_2 = -P_3, \eta_3 = P_1. \quad (2.14b)$$

2.1.4 The Principal Frame

It is of interest to discuss how the Stokes parameters come out in a coordinate frame rotated by an angle ϕ with respect to the xy frame. Of the four Stokes parameters, s_0 and s_3 are frame independent, while s_1 and s_2 are not. Due to the relation (2.11), the parameter $s_\ell > 0$, defined by

$$s_\ell^2 = s_1^2 + s_2^2 \quad (2.15)$$

is also invariant under a frame rotation. It turns out (see Exercise 2.2) that

$$s_1(\phi) = s_1 \cos 2\phi + s_2 \sin 2\phi, \quad (2.16a)$$

$$s_2(\phi) = -s_1 \sin 2\phi + s_2 \cos 2\phi. \quad (2.16b)$$

Thus,

$$\begin{pmatrix} s_0(\phi) \\ s_1(\phi) \\ s_2(\phi) \\ s_3(\phi) \end{pmatrix} = \begin{pmatrix} 1 & 0 & 0 & 0 \\ 0 & \cos 2\phi & \sin 2\phi & 0 \\ 0 & -\sin 2\phi & \cos 2\phi & 0 \\ 0 & 0 & 0 & 1 \end{pmatrix} \begin{pmatrix} s_0 \\ s_1 \\ s_2 \\ s_3 \end{pmatrix}. \quad (2.17)$$

We can now define the principal frame $x'y'$ for the polarization ellipse, i.e., the frame with the x' axis along the major axis of the ellipse, forming an angle γ with respect to the x axis, see Fig. 2.1b. In this frame,

$$s_1(\gamma) = s_\ell, \quad (2.18a)$$

$$s_2(\gamma) = 0. \quad (2.18b)$$

The angle γ , defining the principal frame for the polarization ellipse, may thus be determined from the two equations

$$s_1 = s_\ell \cos 2\gamma, \quad (2.19a)$$

$$s_2 = s_\ell \sin 2\gamma, \quad (2.19b)$$

or, in a single equation, from

$$s_1 + is_2 = s_\ell e^{2i\gamma}. \quad (2.20)$$

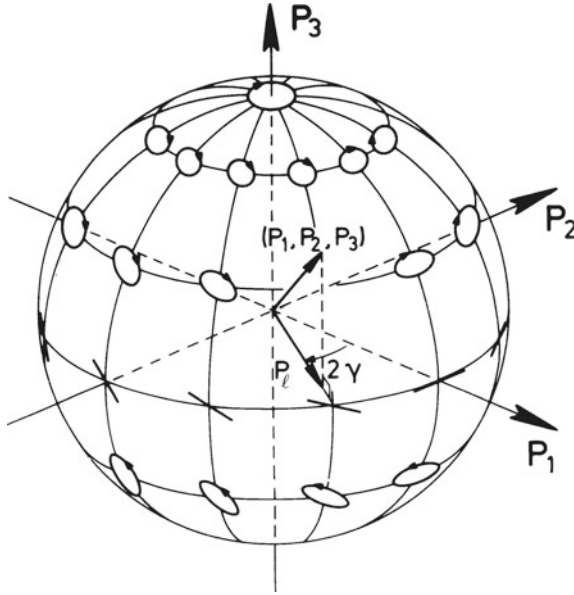


Fig. 2.2 The Poincaré sphere. The Stokes vector (P_1, P_2, P_3) characterizing the polarization ellipse is mapped onto a unit sphere.

2.1.5 The Poincaré Sphere

A useful graphical representation of light polarization was introduced by Poincaré [6]. In this picture, the vector (P_1, P_2, P_3) is visualized as a point on the unit sphere, see Fig. 2.2. Two orthogonal polarizations correspond to opposite points on the unit sphere. For example, the North (South) Pole corresponds to RHC (LHC) polarized light. Furthermore, the equator describes linearly polarized light with γ angle varying with geographical longitude, as shown. Approaching the North Pole from the equator along a meridian corresponds to increasing the degree of circular polarization while keeping the γ angle fixed. For a further discussion of the properties and uses of the Poincaré sphere, see, e.g., [7].

2.2 Electric Dipole Radiation from Atomic Transitions

2.2.1 Coordinate Frames, Scattering Amplitudes, and Stokes Parameters

In this section, we explore the connection between an excited atomic state and the electric dipole radiation pattern, as it is emitted when the state decays to a

lower-lying state. For the sake of simplicity, we first neglect possible effects of electron and nuclear spin (fine and hyperfine structure) and thus assume that the *orbital* angular momentum quantum numbers (LM_L) of the $|nLM_L\rangle$ states involved in the transition completely characterize the radiation pattern.

For symmetry reasons, the radiation pattern from an S state ($L = M_L = 0$) that decays to a P state ($L = 1, M_L = -1, 0, +1$) must be isotropic as long as the magnetic quantum number of the final state is not detected. Hence, the first non-trivial case is the radiation pattern from a P state, which for simplicity we assume will decay to an S state. Simplifying the picture even further, we first analyze the case in which the P-state wavefunction has positive reflection symmetry with respect to a plane. This is a very common case in atomic collisions where the P state is produced by collisional excitation from an S state, also exhibiting positive reflection symmetry with respect to the scattering plane, by a force that conserves reflection symmetry, such as the Coulomb interaction. (See Exercise 2.3 for further discussion.)

The electric dipole radiation pattern is determined by the angular parts of the wavefunctions only. Again, since orbital conventions differ in the literature, we here state explicitly our notation for the spherical harmonics $Y_{LM_L}(\theta, \phi)$ used in the helicity or “atomic physics” basis of ket vectors ($|p_{+1}\rangle, |p_0\rangle, |p_{-1}\rangle$) and the real-valued functions used in the p-orbital or “molecular physics” basis of ket vectors ($|p_x\rangle, |p_y\rangle, |p_z\rangle$).

The corresponding probability densities, i.e., the absolute squares of the wavefunctions, are shown in Fig. 2.3. Omitting the common radial part of the atomic basis functions, we obtain the following dependence on polar angles (θ, ϕ):

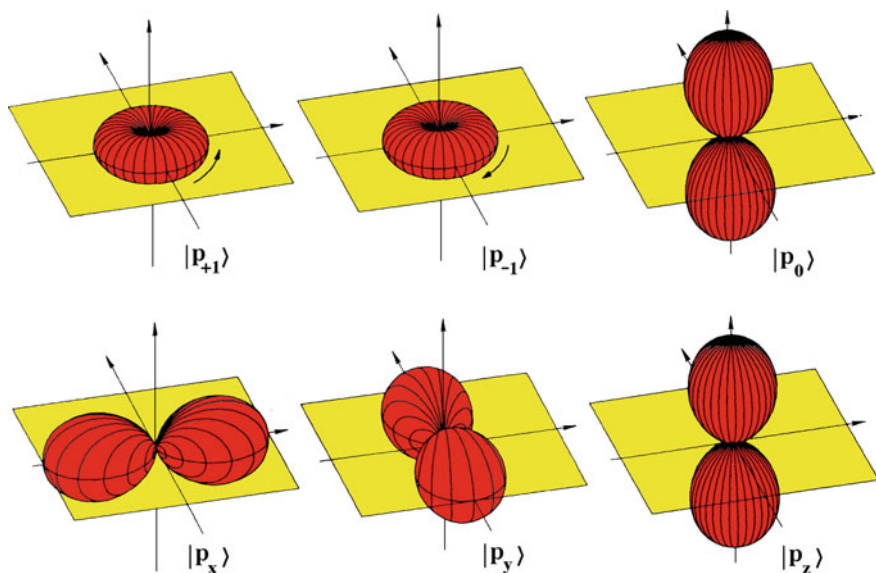


Fig. 2.3 Two sets of P-state basis functions are commonly used. The upper panel shows the probability distributions for the helicity or “atomic physics” basis ($|p_{+1}\rangle, |p_0\rangle, |p_{-1}\rangle$) of (2.23). The lower panel shows the real or “molecular physics” basis ($|p_x\rangle, |p_y\rangle, |p_z\rangle$) of (2.24).

$$\langle \hat{\mathbf{r}} | p_{+1} \rangle = -\sqrt{\frac{3}{8\pi}} \sin \theta e^{i\phi}, \quad (2.21a)$$

$$\langle \hat{\mathbf{r}} | p_0 \rangle = \sqrt{\frac{3}{4\pi}} \cos \theta, \quad (2.21b)$$

$$\langle \hat{\mathbf{r}} | p_{-1} \rangle = \sqrt{\frac{3}{8\pi}} \sin \theta e^{-i\phi}, \quad (2.21c)$$

and

$$\langle \hat{\mathbf{r}} | p_x \rangle = \sqrt{\frac{3}{4\pi}} \sin \theta \cos \phi, \quad (2.22a)$$

$$\langle \hat{\mathbf{r}} | p_y \rangle = \sqrt{\frac{3}{4\pi}} \sin \theta \sin \phi, \quad (2.22b)$$

$$\langle \hat{\mathbf{r}} | p_z \rangle = \sqrt{\frac{3}{4\pi}} \cos \theta. \quad (2.22c)$$

The transformation formulas from one frame to the other are as follows:

$$|p_{+1}\rangle = -\frac{1}{\sqrt{2}}(|p_x\rangle + i|p_y\rangle), \quad (2.23a)$$

$$|p_0\rangle = |p_z\rangle, \quad (2.23b)$$

$$|p_{-1}\rangle = \frac{1}{\sqrt{2}}(|p_x\rangle - i|p_y\rangle), \quad (2.23c)$$

and

$$|p_x\rangle = -\frac{1}{\sqrt{2}}(|p_{+1}\rangle - |p_{-1}\rangle), \quad (2.24a)$$

$$|p_y\rangle = \frac{i}{\sqrt{2}}(|p_{+1}\rangle + |p_{-1}\rangle), \quad (2.24b)$$

$$|p_z\rangle = |p_0\rangle. \quad (2.24c)$$

An orbital's reflection symmetry with respect to the xy plane is determined by its behavior under the mirror operation $\theta \rightarrow \pi - \theta$. From (2.21)–(2.24), we thus see that the orbital $|p_0\rangle = |p_z\rangle$ has negative reflection symmetry, whereas the other ones have positive reflection symmetry.

Two coordinate frames are particularly useful for the discussion of atomic scattering events, cf. Fig. 2.4a. One frame, the so-called *collision frame*, labeled with superscript “c,” has the axis of quantization z^c parallel to the vector \mathbf{k}_{in} of the incoming beam and y^c parallel to $\mathbf{k}_{in} \times \mathbf{k}_{out}$. The other frame, called the *natural frame* and labeled with superscript “n,” has x^n parallel to \mathbf{k}_{in} and the axis of quantization z^n parallel to $\mathbf{k}_{in} \times \mathbf{k}_{out}$. Hence, $x^n = z^c$, $y^n = x^c$, and $z^n = y^c$. Though the outcomes of a specific collision event in the two coordinate frames must be identical, it turns

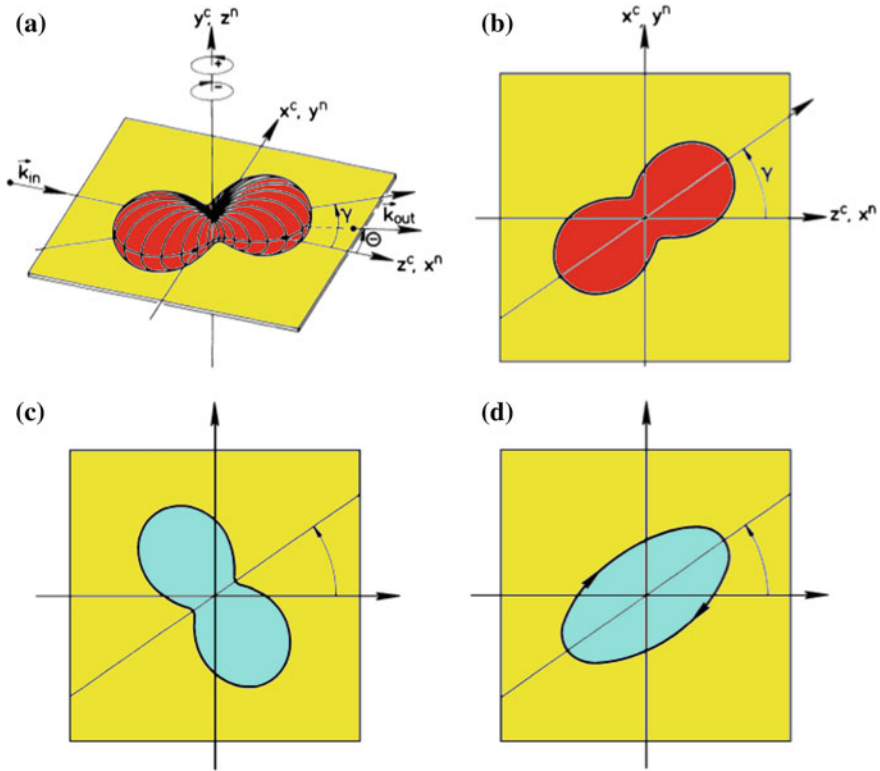


Fig. 2.4 **a** A side view of the angular part of an excited P-state electron charge cloud having positive reflection symmetry with respect to the $x^c z^c = x^n y^n$ scattering plane. **b** A cut through the electron charge cloud in the scattering plane. **c** The angular distribution of photons emitted in the scattering plane. **d** The polarization ellipse for light observed along the direction $+z^n = +y^c$. The case shown has parameters $L_{\perp} = -0.8 \hbar$ and $\gamma = 35^\circ$. See text for the definition of the orientation parameter L_{\perp} and the alignment angle γ .

out that in many cases the algebra becomes simpler and the physics more transparent if the description is performed in the natural frame. (For the *atomic coordinate frame*, see Exercise 2.9.) Since both frames are used in the current literature, we now introduce the fundamental equations in both formulations. The P-state wavefunction $|\psi_P\rangle$ may be expressed as

$$|\psi_P\rangle = f_{+1}^c |p_{+1}^c\rangle + f_0^c |p_0^c\rangle + f_{-1}^c |p_{-1}^c\rangle \quad (2.25a)$$

$$= f_0^c |p_z^c\rangle - \sqrt{2} f_{+1}^c |p_x^c\rangle \quad (2.25b)$$

$$= f_{+1}^n |p_{+1}^n\rangle + f_{-1}^n |p_{-1}^n\rangle \quad (2.25c)$$

$$= -\frac{1}{\sqrt{2}}(f_{+1}^n - f_{-1}^n) |p_x^n\rangle - \frac{i}{\sqrt{2}}(f_{+1}^n + f_{-1}^n) |p_y^n\rangle. \quad (2.25d)$$

Here, we have used (2.23) and the fact (Exercise 2.3) that the assumption of positive reflection symmetry imposes the conditions

$$f_0^n = 0, \quad (2.26a)$$

$$f_{-1}^c = -f_{+1}^c. \quad (2.26b)$$

The coefficients f_{M_L} are the complex probability amplitudes for the individual substates of the three-dimensional subspace spanned by the basis vectors. They are uniquely defined except for a common, arbitrary phase factor. In this chapter, we simply take them for granted. Ways to evaluate them numerically as scattering amplitudes for the collision event of Fig. 2.4a will be summarized in Chap. 6.

Since $|p_z^c\rangle = |p_x^n\rangle$ and $|p_x^c\rangle = |p_y^n\rangle$, we note from (2.25) the following transformation formulas, valid for excitation of P states with positive reflection symmetry:

$$f_0^c = -\frac{1}{2}(f_{+1}^n - f_{-1}^n), \quad (2.27a)$$

$$f_{+1}^c = \frac{i}{2}(f_{+1}^n + f_{-1}^n), \quad (2.27b)$$

and their inverse

$$f_{+1}^n = -\frac{1}{\sqrt{2}}f_0^c - if_{+1}^c, \quad (2.28a)$$

$$f_{-1}^n = \frac{1}{\sqrt{2}}f_0^c - if_{+1}^c. \quad (2.28b)$$

We also read from (2.25) the transformation formulas from the helicity basis (2.21) to the real-values basis (2.22). In the collision coordinate frame, one obtains

$$f_x^c = -\sqrt{2}f_{+1}^c, \quad (2.29a)$$

$$f_y^c = 0, \quad (2.29b)$$

$$f_z^c = f_0^c. \quad (2.29c)$$

Thus, f_{+1}^c and f_0^c are almost the amplitudes in the basis $(|p_x^c\rangle, |p_y^c\rangle, |p_z^c\rangle)$. In the natural coordinate frame one obtains

$$f_x^n = -\frac{1}{\sqrt{2}}(f_{+1}^n - if_{-1}^n), \quad (2.30a)$$

$$f_y^n = -\frac{i}{\sqrt{2}}(f_{+1}^n + if_{-1}^n), \quad (2.30b)$$

$$f_z^n = 0. \quad (2.30c)$$

More useful transformation formulas and general recipes for their derivation are discussed in Chap. 5.

The electric dipole radiation pattern emitted in the $P \rightarrow S$ transition is now readily derived, using the close analogy between the results of the quantum theory of radiation and those from the classical theory of dipole radiation. Equations (2.25b) and (2.25d) correspond to two coherently excited classical dipoles perpendicular to each other with the strengths and phase relations described by the coefficients shown. Defining polarizer angles with reference to the incident beam direction, the Stokes parameters for light emitted in the direction $z^n = y^c$ perpendicular to the scattering plane are thus, except for a common proportionality factor, given by (Exercise 2.4):

$$s_0 = |f_0^c|^2 + 2|f_{+1}^c|^2, \quad (2.31a)$$

$$s_1 = |f_0^c|^2 - 2|f_{+1}^c|^2, \quad (2.31b)$$

$$s_2 = -2\sqrt{2}|f_0^c||f_{+1}^c|\cos\chi, \quad (2.31c)$$

$$s_3 = 2\sqrt{2}|f_0^c||f_{+1}^c|\sin\chi, \quad (2.31d)$$

in terms of the collision frame parameters. Here, χ is the angle from f_0^c to f_{+1}^c in the complex plane,

$$\chi = \arg(f_{+1}^c f_0^{c*}). \quad (2.32)$$

Alternatively, the parameters are given by (Exercise 2.4)

$$s_0 = |f_{+1}^n|^2 + |f_{-1}^n|^2, \quad (2.33a)$$

$$s_1 = -2|f_{+1}^n||f_{-1}^n|\cos\delta, \quad (2.33b)$$

$$s_2 = 2|f_{+1}^n||f_{-1}^n|\sin\delta, \quad (2.33c)$$

$$s_3 = |f_{-1}^n|^2 - |f_{+1}^n|^2, \quad (2.33d)$$

in terms of the natural frame parameters for the helicity basis, where δ is the angle from f_{-1}^n to f_{+1}^n in the complex plane, i.e.,

$$\delta = \arg(f_{+1}^n f_{-1}^{n*}). \quad (2.34)$$

In several cases, particularly for low-energy collisions between heavy particles, the scattering amplitudes in the real-valued basis in the natural coordinate frame ($|p_x^n\rangle, |p_y^n\rangle, |p_z^n\rangle$) are of interest (Exercise 2.4). In this context, the alternative basis labels ($|\sigma\rangle, |\pi^+\rangle, |\pi^-\rangle$) may be found in the literature.

2.2.2 Atomic State Parameters, Electron Charge Clouds, and Their Experimental Determination

For experimental investigation and comparison with theoretical predictions, convenient ways of parameterizing an atomic P state have been introduced. Since the state is completely determined by two complex scattering amplitudes, three real numbers are required for a full characterization (keeping the common, arbitrary phase factor in mind). It is convenient to select these as one cross section and two dimensionless quantities, one relative size and one relative phase.

A natural choice for a cross section is the quantity

$$\sigma = |f_0^c|^2 + 2|f_{+1}^c|^2 \quad (2.35a)$$

$$= |f_{+1}^n|^2 + |f_{-1}^n|^2, \quad (2.35b)$$

i.e., proportional to s_0 , the intensity of light emitted perpendicular to the collision plane.

In the collision frame, the historical choice of dimensionless parameters has been (λ, χ) [8], with the relative size λ , defined as

$$\lambda = \frac{|f_0^c|^2}{\sigma} \quad (2.36)$$

and the relative phase χ given by (2.32). With these definitions, the dimensionless Stokes vector components (2.12) are, according to (2.31) (Exercise 2.5),

$$P_1 = 2\lambda - 1, \quad (2.37a)$$

$$P_2 = -2\sqrt{\lambda(1-\lambda)} \cos \chi, \quad (2.37b)$$

$$P_3 = 2\sqrt{\lambda(1-\lambda)} \sin \chi. \quad (2.37c)$$

In the natural frame, the traditional choice of dimensionless parameters has been (L_\perp, γ) [9]. Here, the relative size is L_\perp , the expectation value of the z^n -component of the transferred orbital angular momentum, i.e.,

$$\frac{\langle \psi_P | \mathbf{L} | \psi_P \rangle}{\langle \psi_P | \psi_P \rangle} = (0, 0, L_\perp), \quad (2.38a)$$

or

$$L_\perp = \frac{|f_{+1}^n|^2 - |f_{-1}^n|^2}{|f_{+1}^n|^2 + |f_{-1}^n|^2}. \quad (2.38b)$$

The alignment angle γ of the polarization ellipse is related to the relative phase angle δ of the scattering amplitudes (2.34) through (Exercise 2.5)

$$2\gamma = \pi - \delta. \quad (2.39)$$

The degree of linear polarization P_ℓ is defined by

$$P_\ell \equiv s_\ell/s_0 = \sqrt{P_1^2 + P_2^2} = \sqrt{1 - P_3^2} = \sqrt{1 - L_\perp^2}. \quad (2.40)$$

It is evidently frame independent.

With these definitions, the dimensionless Stokes vector components (2.12) are obtained from (2.33) (Exercise 2.5):

$$P_1 = P_\ell \cos 2\gamma \quad (2.41a)$$

$$P_2 = P_\ell \sin 2\gamma \quad (2.41b)$$

$$P_3 = -L_\perp. \quad (2.41c)$$

The equation analogous to (2.20) reads

$$P_1 + iP_2 = P_\ell e^{2i\gamma}. \quad (2.42)$$

We thus conclude that the full set of parameters characterizing the P state in the simple case with positive reflection symmetry may be determined by a Stokes vector analysis in the direction perpendicular to the scattering plane. This technique, involving a full determination of the polarization ellipse, is often called *coherence analysis* and may be realized experimentally by using, e.g., scattered-particle-polarized-photon coincidence techniques. These will be further described in Chap. 4.

The wavefunction (2.25) can be written as (Exercise 2.6)

$$|\psi_P\rangle = \sqrt{\frac{\sigma}{2}} \left[\sqrt{1 - P_3} |p_{+1}^n\rangle - \frac{1}{P_\ell} (P_1 + iP_2) \sqrt{1 + P_3} |p_{-1}^n\rangle \right] \quad (2.43a)$$

$$= \sqrt{\frac{\sigma}{2} (1 + L_\perp)} |p_{+1}^n\rangle - e^{2i\gamma} \sqrt{\frac{\sigma}{2} (1 - L_\perp)} |p_{-1}^n\rangle. \quad (2.43b)$$

It is instructive to evaluate the angular part of the P-state electron charge cloud. The result is (Exercise 2.6)

$$|\psi_P|^2(\theta, \phi) = \sigma \frac{1}{2} [1 + P_1 \cos 2\phi + P_2 \sin 2\phi] \sin^2 \theta \quad (2.44a)$$

$$= \sigma \frac{1}{2} [1 + P_\ell \cos 2(\phi - \gamma)] \sin^2 \theta. \quad (2.44b)$$

We may thus associate relative length (ℓ), width (w), and height (h) parameters with the electron cloud, the length being related to the major symmetry axis of the cloud in the collision plane, the width to its minor axis, and the height to the density in the perpendicular direction. We see from (2.44)

$$\ell = \frac{1}{2}(1 + P_\ell), \quad (2.45a)$$

$$w = \frac{1}{2}(1 - P_\ell), \quad (2.45b)$$

$$h = 0, \quad (2.45c)$$

with the normalization

$$\ell + w + h = 1. \quad (2.45d)$$

Note the relation

$$P_\ell = \frac{\ell - w}{\ell + w}, \quad (2.46)$$

which justifies the name *shape parameter* for P_ℓ .

Equation (2.44) was used to generate Fig. 2.4a with $P_\ell = 0.6$ and $\gamma = 35^\circ$. Figure 2.4b shows a cut through the electron charge cloud in the xy plane,

$$|\psi_P|^2(\theta = 90^\circ, \phi) = \frac{1}{2} [1 + P_\ell \cos 2(\phi - \gamma)] \quad (2.47a)$$

$$= \frac{1}{2} [1 + P_1 \cos 2\phi + P_2 \sin 2\phi]. \quad (2.47b)$$

Due to the characteristic properties of electric dipole radiation, this shape can, except for a rotation by 90° , be recorded by a rotatable photon detector tracing the intensity distribution $I(\phi)$ in the direction ϕ in the collision plane, Fig. 2.4c. Hence,

$$I(\phi) = \frac{1}{2} \left[1 + P_\ell \cos 2 \left(\phi - \gamma - \frac{\pi}{2} \right) \right] \quad (2.48a)$$

$$= \frac{1}{2} [1 - P_\ell \cos 2(\phi - \gamma)] \quad (2.48b)$$

$$= \frac{1}{2} [1 - P_1 \cos 2\phi - P_2 \sin 2\phi]. \quad (2.48c)$$

This technique, involving a determination of the shape of the dipole radiation pattern, is called *correlation analysis* and may be realized experimentally by using scattered-particle-emitted-photon coincidence techniques. The radiation emitted in the xy plane will be linearly polarized in this plane, but the detection system need not be sensitive to the polarization. The method has been widely used at wavelengths for which (circular) polarizers are only available with low efficiency, such as the resonance transitions for the rare gases. Correlation analysis may thus extract the parameters (P_1, P_2) or (P_ℓ, γ) , but the sign of L_\perp is left undetermined. The sense of rotation of the electric vector \mathbf{E} of the polarization ellipse, see Fig. 2.4d, is not accessible to detection by this technique.

So far we have neglected the effects of fine and hyperfine structure. Though this is often an excellent approximation during the collision, these internal forces may have ample time to modify the shape and dynamics of the electron charge cloud after the collision, but before the optical decay leading to photon emission takes place. However, using standard techniques (see, e.g., [4]), one can evaluate these effects if the atomic lifetime and the fine and hyperfine coupling constants are known. In this section, we briefly explain the physical effects and postpone the general, quantitative treatment to Chap. 5.

Figure 2.5a shows the time evolution of the electron charge cloud depicted in Fig. 2.4a under the influence of an electron spin of $s = \frac{1}{2}$. The quantum beats are followed through a full period T of the spin precession time ($T = 2\pi/\omega_{fs}$, with $\hbar\omega_{fs} = \Delta E_{fs}$ equal to the fine-structure splitting) and repeat themselves until the optical decay takes place. The depolarizing influence on the time-averaged charge cloud is illustrated by the sequence (b) \rightarrow (c) of Fig. 2.5. The problem can be treated analytically using the tools discussed in Chap. 5. (See also [4] and Appendix B of [10].) The analysis shows that the corresponding effect on the Stokes vector measured in the z'' direction is a reduction in linear polarization, whereas the circular polarization is unaffected. In detail,

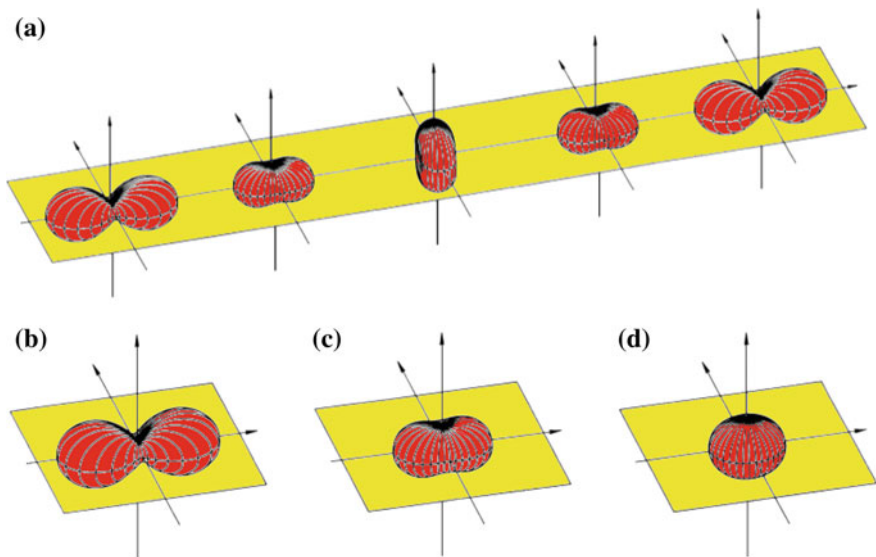


Fig. 2.5 a The time evolution of the shape of the electron charge cloud for an atomic P state with shape parameter $P_\ell = 0.6$ under the influence of spin-orbit coupling for an electron spin $s = \frac{1}{2}$. The five pictures of the quantum beat sequence cover a full precession period and correspond to $\omega_{fs}t = 0, \pi/2, \pi, 3\pi/2$, and 2π , respectively. The sequence repeats itself until the optical decay. The lower row shows the depolarizing influence on the time-averaged charge cloud by (b) \rightarrow (c) an electron spin $s = \frac{1}{2}$, and (c) \rightarrow (d) a nuclear spin $I = \frac{3}{2}$.

$$P_1 \rightarrow \frac{3}{7} P_1, \quad (2.49a)$$

$$P_2 \rightarrow \frac{3}{7} P_2, \quad (2.49b)$$

$$P_3 \rightarrow P_3. \quad (2.49c)$$

It is thus tempting to introduce a so-called *reduced Stokes vector* $\bar{\mathbf{P}}$ with components

$$\bar{P}_1 = \frac{7}{3} P_1, \quad (2.50a)$$

$$\bar{P}_2 = \frac{7}{3} P_2, \quad (2.50b)$$

$$\bar{P}_3 = P_3. \quad (2.50c)$$

to recover the Stokes vector of the *nascent* electron charge cloud. Although the *measured* degree of polarization $P = |\mathbf{P}|$ is generally less than unity, the equation $|\bar{\mathbf{P}}| = 1$ holds for the *reduced* degree of polarization. The sequence (c) \rightarrow (d) of Fig. 2.5 shows the additional depolarizing effect of a nuclear spin of $I = \frac{3}{2}$, as seen, for example, in sodium.

The example above demonstrates the possibility of defining a *reduced* Stokes vector for $P \rightarrow S$ transitions [11] of the form

$$\bar{P}_1 = c_2 P_1, \quad (2.51a)$$

$$\bar{P}_2 = c_2 P_2, \quad (2.51b)$$

$$\bar{P}_3 = c_1 P_3, \quad (2.51c)$$

that corrects for post-collisional fine-structure and hyperfine-structure effects and thus recovers the Stokes vector of the nascent charge cloud, with the degree of polarization being unity.

2.2.3 The Incoherent Case with Conservation of Atomic Reflection Symmetry

Reduction in the degree of polarization may be caused by the experimental setup being unable to distinguish among several, in principle, distinguishable channels, which accordingly will be summed over. An example is impact excitation of sodium by an unpolarized electron beam. Without any knowledge or control of the electron spin, the experiment will add singlet and triplet channels for the total (target + projectile) spin incoherently, and the resulting Stokes parameter will be the weighted sum of the two contributions. An adequate description of such effects is elaborate and will be outlined in Chap. 5; examples will be encountered in Part II.

In the present context, we restrict ourselves to the observation that the resulting Stokes vector is generally no longer a unit vector, i.e., we now have the inequality $P \equiv |\mathbf{P}| \leq 1$ for the degree of polarization. Some authors also introduce the degree of coherence μ [1]. However, since μ depends on the coordinate frame and does not convey any new independent information compared to P , we shall discard it here.

The degree of linear polarization P_ℓ may now be selected as an independent (and coordinate frame independent) parameter. We can thus extract a total of *three* independent, dimensionless parameters from the radiation pattern, namely the set $(L_\perp, \gamma, P_\ell)$.

2.2.4 The Incoherent Case Without Conservation of Atomic Reflection Symmetry

Next, we discuss the case where the assumption of conservation of reflection symmetry of the atomic charge cloud with respect to the collision plane breaks down. This may occur, for example, in electron impact excitation of heavy atoms. Here, the $|p_0^n\rangle$ atomic state may be populated if the electron spin flips, for example, due to spin-orbit coupling. The relative population of the $|p_0^n\rangle$ state is a measure of the relative spin-flip cross section [12], and it can be significant for atoms such as heavy rare gases, or mercury, that we shall encounter in Part II. For these atoms, LS -coupling may no longer be a good description for the excited state. Here, we shall consider the case where the total angular momentum of the excited state is $J = 1$, and the fine structure is completely resolved. Since this state radiates like a set of classical oscillators completely analogous to a 1P_1 state, we shall maintain our previous description, simply replacing the term electron charge cloud density by oscillator density. Also, we keep the traditional notation L_\perp , although J_\perp might seem more appropriate.

We keep the notation from the previous part of this chapter, but modified where necessary with an upper index “+” to indicate parameters related to the part associated with positive reflection symmetry. We thus get

$$L_\perp^+ = -P_3 = \frac{|f_{+1}^n|^2 - |f_{-1}^n|^2}{|f_{+1}^n|^2 + |f_{-1}^n|^2}, \quad (2.52a)$$

$$P_\ell^+ e^{2i\gamma} = P_1 + iP_2 \quad (2.52b)$$

$$P^+ \equiv \sqrt{P_1^2 + P_2^2 + P_3^2} = \sqrt{P_\ell^{+2} + L_\perp^{+2}}. \quad (2.52c)$$

The population of the state (2.21b) with negative reflection symmetry may be described by a probability amplitude f_0^n , and the relative height h of the classical oscillator density will thus be

$$h = \frac{|f_0^n|^2}{\sigma}, \quad (2.53a)$$

now with

$$\sigma = |f_{+1}^n|^2 + |f_0^n|^2 + |f_{-1}^n|^2. \quad (2.53b)$$

In this case, the oscillator density D for the excited atomic state can be written as (Exercise 2.7)

$$D(\theta, \phi) = \sigma \{ (1-h) \frac{1}{2} [1 + P_\ell^+ \cos 2(\phi - \gamma)] \sin^2 \theta + h \cos^2 \theta \}. \quad (2.54)$$

Figure 2.6 shows an example of the effect of a finite height by comparing density plots for $h = 0$ and 0.25, respectively.

The relations (2.45a)–(2.45c) are replaced by

$$\ell = (1-h) \frac{1}{2} (1 + P_\ell), \quad (2.55a)$$

$$w = (1-h) \frac{1}{2} (1 - P_\ell), \quad (2.55b)$$

$$h > 0, \quad (2.55c)$$

with the normalization condition (2.45d) being preserved as

$$\ell + w + h = 1. \quad (2.55d)$$

The relation (2.46) still holds, i.e.,

$$P_\ell^+ = \frac{\ell - w}{\ell + w}. \quad (2.56)$$

In the collision plane, the classical oscillator corresponding to (2.21b) or (2.22c) emits radiation that is polarized perpendicular to this plane. A straightforward experimental approach to use for determination of its relative strength is thus to determine the Stokes vector corresponding to a direction *in* the collision plane perpendicular to the beam, i.e., along the y^n direction. This will have the form $(P_4, 0, 0)$, the two last components being zero for symmetry reasons. The parameter h may then be determined from the equation (Exercise 2.8)

$$h = \frac{(1 + P_1)(1 - P_4)}{4 - (1 - P_1)(1 - P_4)}. \quad (2.57)$$

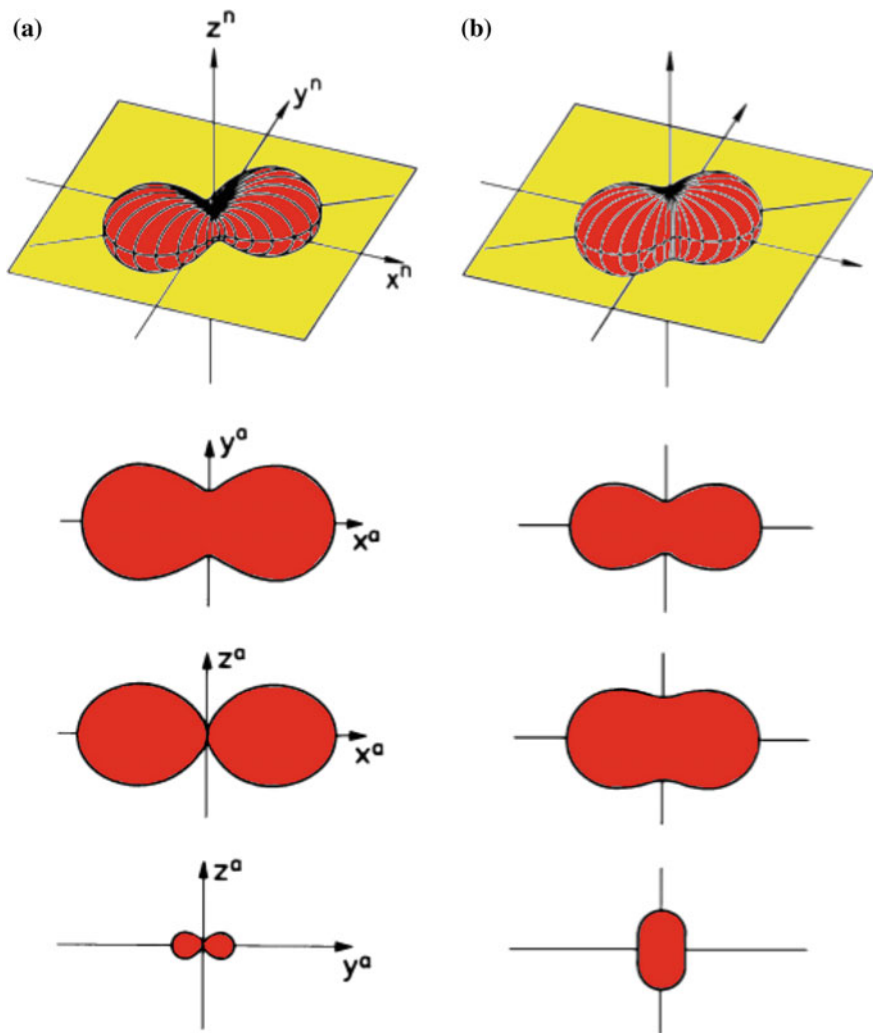


Fig. 2.6 The top row shows classical oscillator densities with linear polarization $P_\ell = 0.6$ and alignment angle $\gamma = 35^\circ$. The height parameter is $h = 0$ (a) and 0.25 (b), respectively. Shown below are cuts along the principal planes of the densities.

In the general case of a $J = 1 \rightarrow J_f = 0$ transition, therefore, *four* parameters, conveniently selected as $(L_\perp^+, \gamma, P_\ell^+, h)$, can be extracted from the radiation pattern. Observation from *two* directions is required for their determination. Alternatively, the parameter h may be derived from a correlation analysis by an additional measurement involving a direction out of the collision plane. (See Sect. 3.3.1 of [10] for a quantitative evaluation of this approach.)

Table 2.1 Summary of cases of increasing complexity and the orientation and alignment parameters necessary for characterization. The table is valid for unpolarized beams only.

Example case	e–He	e–Na	e–Hg
Forces	Coulomb	+ exchange	+ spin-orbit
Representation	wavefunction	density matrix	density matrix
Reflection symmetry	+	+	+, –
Parameters			
Angular momentum	L_{\perp}	L_{\perp}	L_{\perp}^{+}
Alignment angle	γ	γ	γ
Linear polarization	P_{ℓ}	P_{ℓ}	P_{ℓ}^{+}
Degree of polarization	$P = 1$	$P \leq 1$	$P^{+} \leq 1$
Height	$h = 0$	$h = 0$	$h \geq 0$
Independent parameters	2	3	4
Observation directions	1	1	2

2.2.5 Summary of Parameterization for P-State Excitation

The results of the preceding sections are summarized in Table 2.1. The table gives the three cases of increasing complexity, summarizing their reflection symmetry with respect to the scattering plane, the maximum number of independent alignment and orientation parameters, their definitions, and the number of observation directions necessary for a full characterization of the radiation pattern. The top line lists some collision systems that belong to the three categories, respectively, together with the forces active during the excitation process.

The discussion may be generalized further to states with $L > 1$. Already the case of D-state excitation becomes considerably more involved, but the theory and notation can be developed as a natural extension of the framework outlined above. A number of theoretical and experimental papers have addressed this problem, which requires triple-coincidence techniques for full elucidation [13, 14]. At the time of writing, collisional excitation of F-states or states with even higher angular momentum has, except for a few pioneering studies [15–17], been addressed at the level of total, or scattering-angle integrated, cross sections and polarizations — concepts to be discussed systematically in the following chapter.

2.2.6 Extension to Coherently Excited Stark Manifolds

The above discussion can be extended in several ways, some of which will also be discussed in Part 2 of this book. Here, we mention one case, in which the degeneracy of pure Coulombic systems plays an important role. Specifically, we summarize the

treatment outlined in [18] for coherent excitation of the 2s and 2p states in one-electron systems from the 1s state.

In addition to the two amplitudes for the 2p state, excitation to the 2s state is described by a single scattering amplitude f_s . For the discussion below, it is advantageous to also introduce the “molecular-orbital” basis states in the natural coordinate system. As shown above, these are related to the $|m = \pm 1\rangle$ states through

$$|x\rangle = -\frac{1}{\sqrt{2}} (|+1\rangle - |-1\rangle), \quad (2.58a)$$

$$|y\rangle = \frac{i}{\sqrt{2}} (|+1\rangle + |-1\rangle), \quad (2.58b)$$

and the corresponding amplitudes are

$$f_x = -\frac{1}{\sqrt{2}} (f_{+1} - f_{-1}), \quad (2.59a)$$

$$f_y = -\frac{i}{\sqrt{2}} (f_{+1} + f_{-1}). \quad (2.59b)$$

Figure 2.7 shows the three amplitudes f_s , f_x , and f_y as complex numbers, each one being represented by its magnitude and phase. Recall, however, that only the relative phases can be determined experimentally.

A typical angle-differential cross section experiment would measure the sum of the cross sections for excitation of the $n=2$ state manifold, i.e.,

$$\sigma \equiv \sigma_s + \sigma_p = |f_s|^2 + |f_{+1}|^2 + |f_{-1}|^2 = |f_s|^2 + |f_x|^2 + |f_y|^2. \quad (2.60)$$

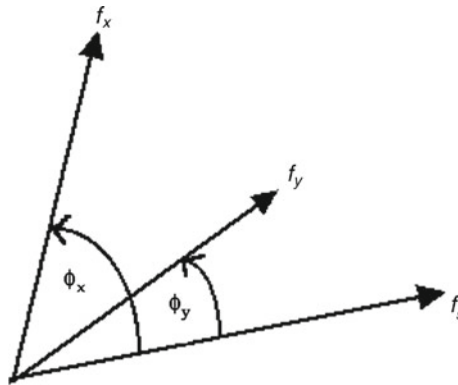


Fig. 2.7 The scattering amplitudes for coherent excitation of $1s \rightarrow 2s$ and $1s \rightarrow 2p$. (From [18].)

A thorough analysis of this problem can be found in [18], to which we refer for further details. Briefly, the purely Coulombic case offers the unique opportunity to probe not only the amplitudes $f_{\pm 1}$ (relative magnitude and phase) by Stokes parameter analysis of the decay photon, but also f_s and the relative phase between the amplitudes for excitation of the 2s and 2p states. This can be achieved by introducing an electric field in the scattering plane, which will result in a mixture of the two different-parity 2s and 2p states through the Stark effect. Consequently, the charge cloud representing the coherently excited $n=2$ states will generally exhibit a dipole moment. Thus, by applying an electric field, it will be possible to tell, e.g., on which side of the nucleus the excited electron is more likely to be located.

As shown in [18], the “normalized” charge cloud density can be expressed as

$$C(r, \theta, \phi) = \frac{1}{4\pi} \left[w_s R_{20}^2(r) + \frac{3}{2} w_p R_{21}^2(r) \sin^2 \theta (1 + P_\ell \cos 2(\phi - \gamma)) \right. \\ \left. + \sqrt{3} R_{20}(r) R_{21}(r) \sin \theta D \cos(\phi - \varepsilon) \right] \quad (2.61a)$$

$$\equiv C_{2s} + C_{2p} + C_{sp}, \quad (2.61b)$$

with

$$w_s \equiv \sigma_s / (\sigma_s + \sigma_p) \quad (2.62a)$$

and

$$w_p \equiv \sigma_p / (\sigma_s + \sigma_p) \quad (2.62b)$$

representing the relative weights of the excitations to the 2s and the 2p states. Furthermore, we have used the standard hydrogenic radial functions $R_{n\ell}(r)$ and defined D , P_ℓ , ε , and γ by

$$D_x + i D_y \equiv D e^{i\varepsilon}, \quad (2.63a)$$

$$P_1 + i P_2 \equiv P_\ell e^{2i\gamma} \quad (2.63b)$$

with D , $P_\ell \in [0, 1]$, $\varepsilon \in [0, 2\pi]$, and $\gamma \in [-\frac{\pi}{2}, \frac{\pi}{2}]$. Here,

$$\mathbf{D} = \frac{\langle \Psi | e \mathbf{r} | \Psi \rangle}{\langle \Psi | \Psi \rangle} = -\frac{3a_0 e}{Z} (D_x, D_y, 0) \quad (2.64)$$

is the dipole moment with its two components, e is the elementary charge, a_0 is the Bohr radius, and Z is the nuclear charge number.

A *complete* experiment for such a process then requires the determination of three complex scattering amplitudes, i.e., three magnitudes and two relative phases (see Fig. 2.2). This information can be obtained in a three-step process: (i) measurement of the absolute TDCS, $\sigma = \sigma_s + \sigma_p$; (ii) field-free Stokes parameter analysis of the 2p component, providing (L_\perp, γ) ; and (iii) Stokes parameter analysis of the Stark-quenched 2p component as function of external electric field strength, for example, by adapting the procedure of [19,20]. The latter step may provide the observables (w_s, D, ε) . Note that w_s will determine the individual absolute cross sections σ_s and σ_p , respectively.

Exercises

- 2.1 Derive the four equations (2.10) from (2.9) and the definitions of the Stokes vectors.
- 2.2 Show (2.16) for the Stokes parameters in a rotated frame.
- 2.3 Consider the conservation of positive reflection symmetry.
 - (a) What are the reflection symmetries of the three P-state components in the “atomic physics basis” (2.21) and in the “molecular physics basis” (2.22)?
 - (b) Prove that conservation of positive reflection symmetry for $S \rightarrow P$ excitation leads to (2.26).
 - (c) Generalize (a) to the basis sets for D states.
- 2.4 Generate expressions for the Stokes parameters of excited P states.
 - (a) Derive (2.31) for the collision coordinate frame.
 - (b) Derive (2.33) for the atomic physics basis in the natural coordinate frame.
 - (c) Derive expressions for the Stokes parameters using the natural coordinate frame and the molecular physics basis $(|p_x^n\rangle, |p_y^n\rangle, |p_z^n\rangle)$ and compare to (2.31).
- 2.5 Express the Stokes parameters in terms of the P-state parameters.
 - (a) Derive (2.37) for the collision coordinate frame.
 - (b) Derive (2.41) and (2.42) for the natural coordinate frame in the atomic physics basis.
- 2.6 Prove (2.43) for the P-state wavefunction in terms of the Stokes vector components.
- 2.7 Discuss the loss of positive reflection symmetry for the atomic $J = 1$ state. In (2.54), the two parts of the wavefunction with positive and negative reflection symmetry have been added incoherently. Why is this procedure valid?
- 2.8 Derive the relation (2.57) for the height parameter h by evaluating the linear polarizations P_1 and P_4 for emission from three orthogonal classical oscillators aligned along the x , y , z axes.
- 2.9 The atomic coordinate frame (x', y', z') is obtained from the natural frame by rotation through the angle γ around the $z = z'$ axis. Hence, the $x'y'$ coordinate frame is the principal frame of the polarization ellipse.

- (a) Translate the formulas (2.43) and (2.44) into atomic-frame parameters using (i) the helicity basis ($|p_{+1}\rangle, |p_0\rangle, |p_{-1}\rangle$) and (ii) the real-valued basis ($|p_x\rangle, |p_y\rangle, |p_z\rangle$).
- (b) Establish transformation formulas that relate scattering amplitudes in the atomic frame to those in the collision frame and the natural frame.

References

1. M. Born, E. Wolf, *Principles of Optics*, 4th edn. (Pergamon Press, New York, 1970)
2. G.G. Stokes, Trans. Cambr. Phil. Soc. **9** (1852) 399. Reprinted in: *Mathematical and Physical Papers*, Vol. III, Cambridge University Press 1901, p. 233
3. E.B. Brown, *Modern Optics* (Reinhold Publication Corp, New York, 1965)
4. K. Blum, *Density Matrix Theory and Applications*, 3rd edn. (Springer, New York, 2012)
5. J. Kessler, *Polarized Electrons*, 2nd edn. (Springer, Heidelberg, 1985)
6. H. Poincaré, *Théorie Mathématique de la Lumière* (Chap. 12), G. Carré, Paris 1889
7. W.A. Shurcliff, *Polarized Light: Production and Use* (Harvard University Press, Harvard, 1962)
8. M. Eminyan, K.B. MacAdam, J. Slevin, M.C. Standage, H. Kleinpoppen, J. Phys. B **7**, 1519 (1974)
9. N. Andersen, I.V. Hertel, H. Kleinpoppen, J. Phys. B **17**, L901 (1984)
10. N. Andersen, J.W. Gallagher, I.V. Hertel, Phys. Rep. **165**, 1 (1985)
11. N. Andersen, T. Andersen, C.L. Cocke, E.H. Pedersen, J. Phys. B **12**, 2541 (1979)
12. N. Andersen, K. Bartschat, G.F. Hanne, J. Phys. B **28**, L29 (1995)
13. N. Andersen, K. Bartschat, J. Phys. B **30**, 5071 (1997)
14. A.G. Mikosza, J.F. Williams, J.B. Wang, Phys. Rev. Lett. **79**, 3375 (1997)
15. D. Cvejanovic, A. Crowe, Phys. Rev. Lett. **80**, 3033 (1998)
16. D.V. Fursa, I. Bray, Phys. Rev. A **59**, 1297 (1999)
17. J.B. Wang, C.M. Maloney, D.H. Madison, J. Phys. B **32**, 1067 (1999)
18. N. Andersen, K. Bartschat, J. Phys. B **37**, 3809 (2004)
19. J.R. Ashburn, R.A. Cline, C.D. Stone, P.J.M. van der Burgt, W.B. Westerveld, J.S. Risley, Phys. Rev. A **40**, 4885 (1989)
20. R.A. Cline, P.J.M. van der Burgt, W.B. Westerveld, J.S. Risley, Phys. Rev. A **49**, 2613 (1994)

<http://www.springer.com/978-3-319-55214-9>

Polarization, Alignment, and Orientation in Atomic Collisions

Andersen, N.; Bartschat, K.

2017, XXIII, 404 p. 237 illus., 39 illus. in color.,

Hardcover

ISBN: 978-3-319-55214-9